This article has been accepted for publication in a future issue of this journal, but has not been fully edited. Content may change prior to final publication. Citation information: DOI 10.1109/TPWRD.2015.2464323, IEEE Transactions on Power Delivery

SSR Damping in Fixed-Speed Wind Farms using Series FACTS Controllers

Hossein Ali Mohammadpour, *Student Member, IEEE*, Md Moinul Islam, *Student Member, IEEE*, Enrico Santi, *Senior Member, IEEE*, Yong-June Shin, *Senior Member, IEEE*

***Abstract*—Sub-synchronous resonance (SSR) damping in fixed-speed wind turbine generator systems (FSWTGS) by using two series flexible AC transmission system (FACTS) devices, the thyristor-controlled series capacitor (TCSC) and gate-controlled series capacitor (GCSC), is studied in this paper. The former is a commercially available series FACTS device, and the latter is the second generation of series FACTS devices uses gate turn-off (GTO) or other gate commuted switches. The GCSC is characterized by a fixed-capacitor in parallel with a pair of anti-parallel gate-commuted switches enabling rapid control of series impedance of a transmission line. It is shown that the SSR damping with a GCSC is limited to changing the resonance frequency, in comparison with a fixed capacitor, which may not be adequate to damp out the SSR. Therefore, a supplementary SSR damping controller (SSRDC) is designed for the GCSC. Moreover, it is proven that the GCSC equipped with a well-designed SSRDC can effectively damp the SSR in FSWTGS. In order to verify the effectiveness of the GCSC in SSR damping, its performance is compared with the TCSC, which is an existing series FACTS device. In addition, time-frequency analysis (TFA) is employed in order to evaluate and compare the SSR time-varying frequency characteristics of the GCSC and TCSC. The IEEE first benchmark model on SSR is adapted with an integrated FSWTGS to perform studies, and the extensive simulations are carried out using PSCAD/EMTDC to validate the result.**

***Index Terms*—Fixed-speed wind turbine, sub-synchronous resonance, wind farm, FACTS, power quality, gate-controlled series capacitor (GCSC), TCSC, time-frequency analysis.**

I. Introduction

POSSIBLE shortage of conventional fossil fuels and environmental pollution are two of the most important energy-related issues that the world is facing today [1] - [2]. These issues have led to increasing interest in electric power generation by renewable energy sources, specially wind power [3] - [5]. The two primary types of wind turbine generator systems (WTGS) are fixed-speed wind turbine generator systems (FSWTGS) and variable speed WTGS [6].

Part of this paper was presented at 4th IEEE International Symposium on Power Electronics for Distributed Generation Systems (PEDG) 2013, 8 - 11 July, Rogers, AR, USA. This work was supported by the National Science Foundation (NSF) I/UCRC (Industry/University Cooperative Research Center) for Grid-Connected Advanced Power Electronic Systems (GRAPES) center, under #0934378. This research was also supported by Korea National Research Foundation under #NRF-2012M2A8A4055236 and #NRF-2014R1A2A1A01004780.

Corresponding Author: Yong-June Shin (e-mail: yongjune@yonsei.ac.kr).

H. A. Mohammadpour is with NRG Renew, Scottsdale, AZ, 85251 USA.

Md Moinul Islam, and E. Santi are with the Department of Electrical Engineering, University of South Carolina, Columbia, SC, 29208 USA.

Y.-J. Shin is with the School of Electrical and Electronic Engineering, Yonsei University, Seoul 120-749, Korea.

Because of increased integration of wind farms into electric power grids, it is necessary to transmit the generated power from wind farms to the existing grids via transmission networks without congestion. Moreover, in the deregulated power market, it is necessary to increase the power transfer capability of existing transmission lines at the lowest cost [7]. Series capacitive compensation of wind farms is an economical way to increase the power transfer capability of the transmission line connecting wind farm to the grid.

Nevertheless, sub-synchronous resonance (SSR) is a potential risk in series compensated wind farms [8]. The SSR can be divided into two main categories, namely induction generator effect (IGE), and torsional interactions (TI). While the IGE solely involves the electrical part of the system and its interaction between the electrical network and the generator, the TI effect involves both the electrical and mechanical parts of the overall system [9] - [10]. In the wind farms interfaced with series compensated network, the IGE due to the network resonance oscillatory mode is the major cause of the SSR [11]. Because of the low shaft stiffness of the wind turbine drive train, the frequency of torsional modes in wind turbines is in the range of 1 to 3 Hz so that in order to cause TI, a very high level of series compensation is required, which rarely happens [11]. Therefore, this paper considers only the IGE effect.

Although mitigation of the SSR by control of FACTS devices is well-known in traditional power systems, their application in wind farms requires additional analysis. References [11] - [13] and [8] present modeling and stability analysis of doubly-fed induction generator (DFIG)-based wind farms interfaced to the grid with a series compensated transmission line. Reference [14] also presents the potential use of supplemental control of DFIG-based wind farms for damping SSR oscillations in nearby turbine-generators connected to series compensated transmission systems. References [15] and [16] also study the SSR mitigation in wind farms using STATCOM.

Thyristor controlled series capacitor (TCSC) has been utilized for series compensation of transmission lines [10]. This device consists of a thyristor-controlled reactor (TCR) in parallel with a fixed capacitor for each phase, which is a later member of the first generation of FACTS devices. The world's first TCSC was manufactured and installed at Kayenta substation, Arizona in 1992. The TCSC installed at Kayenta substation increased the transmittable power capacity of the transmission line to approximately 30% [17] - [19].

Because of its simplicity compared to other more complex and expensive FACTS devices such as STATCOM and TCSC [20], the gate controlled series capacitor (GCSC) can be of

0885-8977 (c) 2015 IEEE. Personal use is permitted, but republication/redistribution requires IEEE permission. See http://www.ieee.org/publications_standards/publications/rights/index.html for more information.

This article has been accepted for publication in a future issue of this journal, but has not been fully edited. Content may change prior to final publication. Citation information: DOI 10.1109/TPWRD.2015.2464323, IEEE Transactions on Power Delivery

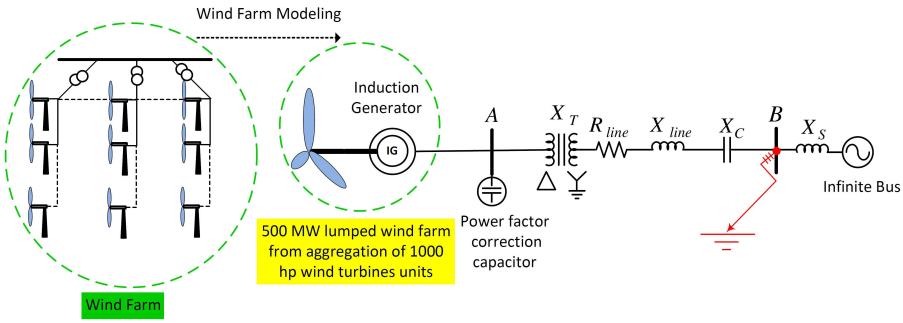

Fig. 1. One line diagram of the studied power system: X_T Transformer reactance, R_{line} Transmission line resistance, X_{line} Transmission line reactance, X_C Fixed series capacitor, X_S System impedance

more interest for real-world applications in future electric power systems. This device is characterized as a series FACTS device which was initially proposed for series compensation of a transmission line to control power flow [20] - [21]. In [20] and [22] - [24], the application of the GCSC has been studied for SSR damping in traditional power systems. In [20] , [22] a constant power controller is implemented to the GCSC to damp the SSR. In [23], [24], a constant power controller is modified with a fuzzy logic controller to enable the GCSC to damp the SSR. However, as it will be shown in this paper, the effect of the GCSC is only to modify the effective value of its capacitance to change the resonance frequency as compared to a fixed capacitor. Therefore, a constant power controller, even modified with a fuzzy controller, may not be adequate to damp the SSR, and an auxiliary controller should be used as a supplementary controller to mitigate the SSR.

The authors of the current work presented some preliminary results in [25] about the application and control of the GCSC to damp the SSR in fixed speed wind farms. However, this problem still requires a detailed analysis, including analysis and design of the grid-connected GCSC SSR damping controller, verifying the effectiveness of the GCSC's transient performance using a commercially available FACTS device such as the TCSC, and employing the time-frequency technique for SSR analysis, which is presented in this paper.

This paper proposes the application and control of the GCSC for SSR damping in FSWTGS. It will be shown that a power scheduling controller (PSC) is not sufficient to damp the SSR. Therefore, in order to achieve an effective SSR damping, a supplementary SSR damping controller (SSRDC) is added to the PSC. In order to verify the effectiveness of the GCSC, its performance is compared with a well-known series FACTS device, the TCSC. The power system considered in this paper is a modified version of the IEEE first benchmark model for computer simulation of SSR [26]. Time domain simulations are carried out using PSCAD/EMTDC [27].

Moreover, it is not an easy task to assess improvement of the power quality with mitigation devices. Fast Fourier transform (FFT) has been utilized to evaluate the effectiveness of SSR damping controllers [28] - [29], which is based on traditional Fourier analysis [30]. The FFT assumes a disturbances of a periodic nature. The SSR, however, can be characterized as non-stationary in nature. Therefore, time-frequency based power quality index [31] - [32] using time-frequency analysis (TFA) is applied to determine how the spectral components (consisting of the fundamental and SSR frequencies) of the line current vary in time. Using these results, the performance of the GCSC for SSR damping is compared to that of the TCSC.

New contributions of the paper are summarized as follows:

1) application of the GCSC for SSR damping in fixed-speed wind farms
2) comparing the GCSC performance in SSR damping with a commercially available FACTS device, TCSC
3) using the time-frequency analysis to evaluate the performance of FACTS devices, GCSC and TCSC, in SSR damping.

The organization of the rest of the paper is as follows. In Section II, the studied power system and the SSR in wind farms are briefly described. In Section III, the GCSC and its analysis for SSR studies are presented. In Section IV, the GCSC control system, including power scheduling controller and SSR damping controller are explained. In Section V, the results and discussion are presented in order to validate the SSR damping controller design for the GCSC. In this section, the performance of the GCSC is compared with the performance of the TCSC in SSR damping using both time-domain simulations and time-frequency technique. Finally, Section VI concludes the work.

II. Studied System Model

Fig. 1 shows the test system, where a 500 MW FSWTGS-based wind farm is connected to the infinite bus through a 500-kV series compensated transmission line. We assume that the wind farm aggregation provides a reasonable equivalent model for the system studies [33]. Therefore, the wind farm in this paper is created from the aggregation of large number, 670 of 1000-hp self-excited double-cage IGs [27]. Most of the commercially operated IGs, whose nominal power is more than 5 kW, have a double-cage rotor [34]. Compared to single-cage machines, double-cage machines are widely used in wind farms, since the slip in these machines can vary over a wide range [35]. Therefore, a double-cage IG-based wind turbine is considered in this paper.

0885-8977 (c) 2015 IEEE. Personal use is permitted, but republication/redistribution requires IEEE permission. See http://www.ieee.org/publications_standards/publications/rights/index.html for more information.

This article has been accepted for publication in a future issue of this journal, but has not been fully edited. Content may change prior to final publication. Citation information: DOI 10.1109/TPWRD.2015.2464323, IEEE Transactions on Power Delivery

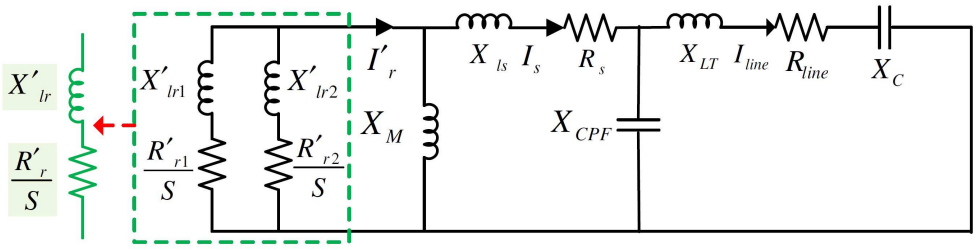

Fig. 2. Equivalent circuit diagram of a FSWTGS under sub-synchronous resonance frequency: R'_{r1}, R'_{r2}: first and second cage resistance, X'_{lr1}, X'_{lr2}: first and second cage reactance, X_{ls} stator leakage reactance, R_s stator resistance, X_M magnetizing reactance, $X_{LT} = X_{line} + X_T + X_S$, I_s stator current, I_r rotor current, X_C series capacitor.

Since the IG lacks an external exciter, a shunt capacitor is added to the wind farm bus to bring up the power factor to approximately 0.98-0.99 lagging. The transmission line in this study is derived from the IEEE first benchmark model for SSR studies [26].

A series compensated power system with a compensation level defined as $K = \frac{X_C}{X_{LT}}$ excites sub-synchronous currents at frequency given by [10]:

$$f_n = f_s \sqrt{\frac{K X_{LT}}{\sum X}} \tag{1}$$

where X_C is the fixed series capacitor, $X_{LT} = X_{line} + X_T$, f_s is the frequency of the system (Hz), and f_n is the natural frequency of the system (Hz).

Moreover, $\sum X$ is the entire reactance seen from the infinite bus and is obtained as follows:

$$\sum X = X'_{lr} + X_{ls} + X_{LT} \tag{2}$$

where X'_{lr}, X_{ls}, and X_{LT} are defined in Fig. 2.

At the frequency f_n, the slip, given by (3), becomes negative since the natural resonance frequency, f_n, is less than the electric frequency corresponding to the rotating speed, f_m.

$$S = \frac{f_n - f_m}{f_n} \tag{3}$$

The steady state equivalent circuit of the system under sub-synchronous frequency is shown in Fig. 2. The values of the magnetizing reactance X_M and the power factor correction capacitor X_{CPF} are large compared to the other elements of the equivalent circuit of the system shown in Fig. 2 so that they can be neglected. If the magnitude of the equivalent rotor resistance exceeds the sum of the resistances of the armature and the network, there will be a negative resistance at the sub-synchronous frequency, and the sub-synchronous current would increase with time. This phenomenon is called induction generator effect (IGE) [9], and only involves rotor electrical dynamics [12].

A. Fixed-Series Compensation (FSC)

In this section, the IGE effect is investigated in the absence of a GCSC device in the system model shown in Fig. 1, and the system operates under FSC only. Fig. 3 shows the impedance profile of the system seen from infinite bus at Fig. 1. As seen in this figure, the series compensation results in a resonance at frequencies 26.83, 37.94, 46.47, and 49.45 Hz for the compensation levels $K = 20\%, 40\%, 60\%, 70\%$, respectively. Notice that practical series compensation is not normally more than 70% - 75% for the reasons such as load balancing with parallel paths, high fault current, and the possible difficulties of power flow control [36]. Therefore, in this paper, the maximum compensation is limited to 70%.

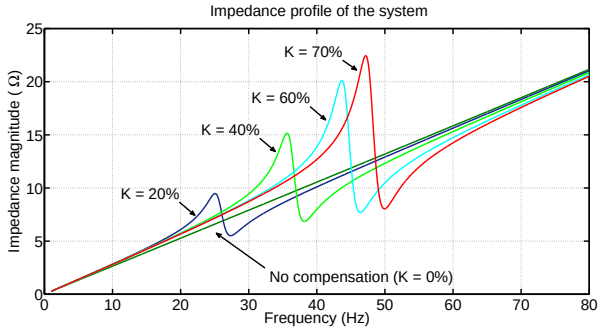

Fig. 3. Impedance profile of the system for different series compensation levels, $K = 0\%, 20\%, 40\%, 60\%, 70\%$.

The simulation of the wind farm starts with 30% series compensation, and then at $t = 1$ $sec.$, the compensation increases to 50%, 60%, and 68%, respectively. Fig. 4. (a) - (c) show the electric torque of the induction generator (IG). From Fig. 4 (a) and (b), it is clear that the increase of the compensation level from 30% to 50% and 60%, sub-synchronous oscillations appear in the electric torque, and these oscillations decay with time. However, as shown in Fig. 4 (c), when compensation level is increased to 68%, the sub-synchronous oscillation with dominant frequency of 9.5 Hz - which is the complement of the electric natural frequency f_n given in (1) for $K = 68\%$ and can be obtained using Fig. 3 - appears in the electric torque, and it does not decay with time, which leads to instability of the wind farm.

III. Gate-Controlled Series Capacitor (GCSC)

A. Structure of the GCSC

A GCSC (one per phase), as shown in Fig. 5, consists of a fixed-capacitor in parallel with a pair of anti-parallel switch

0885-8977 (c) 2015 IEEE. Personal use is permitted, but republication/redistribution requires IEEE permission. See http://www.ieee.org/publications_standards/publications/rights/index.html for more information.

This article has been accepted for publication in a future issue of this journal, but has not been fully edited. Content may change prior to final publication. Citation information: DOI 10.1109/TPWRD.2015.2464323, IEEE Transactions on Power Delivery

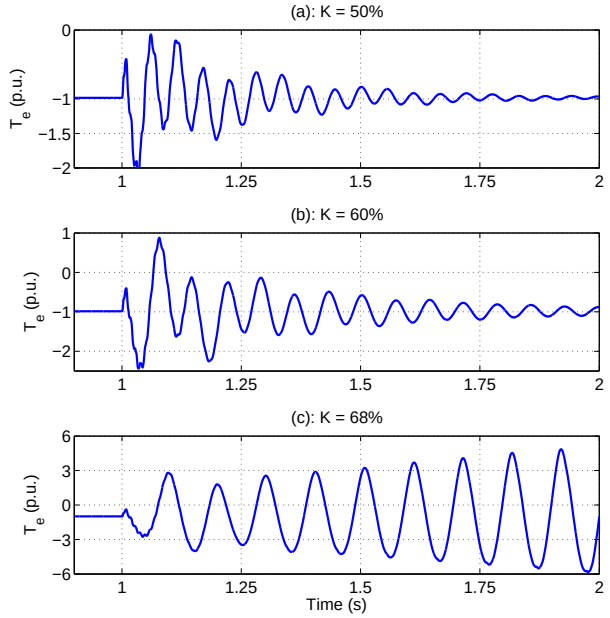

Fig. 4. Electric torque of wind farm for different fixed series compensation levels, K: (a) $K = 50\%$, (b) $K = 60\%$ (c) $K = 68\%$.

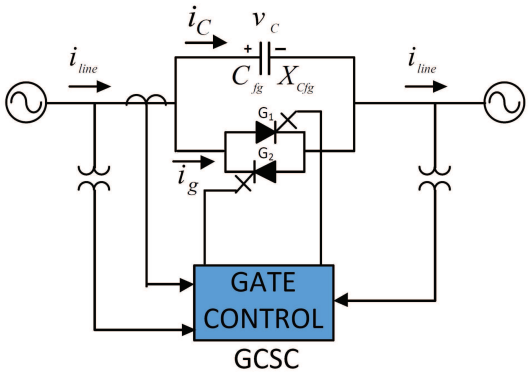

Fig. 5. Single line configuration of the GCSC: $i_{line}(t)$ Transmission line current, $i_C(t)$ GCSC's capacitor current, $i_g(t)$ GTO current, v_C Voltage across the GCSC, X_{Cfg} Fixed capacitance of the GCSC.

made up of a pair of GTO thyristors. In contrast to a thyristor, a GTO thyristor can be turned off upon command. The switch in the GCSC is turned off at an angle γ, measured from the peak value of the line current, i_{line}. When the GTO switch across the capacitor is turned off at an angle γ, the line current is forced to flow through the capacitor and the voltage $v_C(t)$ appears across the GCSC.

The effective capacitance of the GCSC is given by [24]:

$$X_G = X_{Cfg}(1 - \frac{2\gamma}{\pi} - \frac{\sin 2\gamma}{\pi}) = \frac{X_{Cfg}}{\pi}(2\beta - \sin 2\beta) \quad (4)$$

where γ is GCSC turn-off angle ($rad.$), and β is the angle of the advance ($rad.$).

When $\gamma = 0$ or $\beta = \frac{\pi}{2}$, the capacitor is continuously conducting, and when $\gamma = \frac{\pi}{2}$ or $\beta = 0$, the capacitor voltage is zero as the capacitor is totally bypassed by the GTO switches.

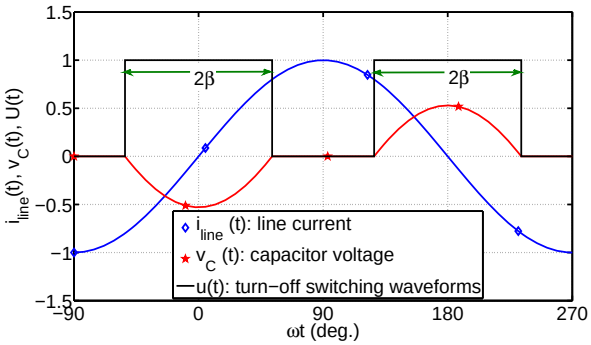

Fig. 6. Line current, capacitor voltage, and switching function of the GCSC.

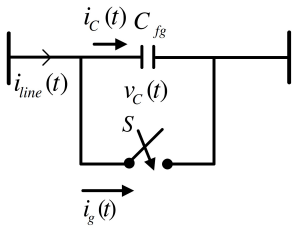

Fig. 7. GCSC circuit.

B. Analysis of SSR Using GCSC

Fig. 6 shows line current, capacitor voltage and switching function in a GCSC. Also, the circuit of the GCSC can be considered as shown in Fig. 7. The voltage across the GCSC's capacitor can be expressed as:

$$\frac{dv_C(t)}{dt} = \frac{i_C(t)}{C_{fg}} \quad (5)$$

where $i_C(t)$ is:

$$i_C(t) = i_{line}(t) - i_g(t) \quad (6)$$

$i_g(t)$ can be expressed as:

$$i_g(t) = (1 - u(t))i_{line}(t) \quad (7)$$

where $u(t)$ is the switching function waveforms in the GCSC shown in Fig. 6 so that $u = 1$, when the switch is open, and $u = 0$, when the switch is closed. Note that in the GCSC, the switching function, $u(t)$, is the turn-off switching pulses.

Substituting Eq. (7) in Eq. (6) results in:

$$i_C(t) = u(t)i_{line}(t) \quad (8)$$

Substituting Eq. (8) in Eq. (5) results in:

$$C_{fg}\frac{dv_C(t)}{dt} = u(t)i_{line}(t) \quad (9)$$

In general, using Fourier series, $u(t)$ can be approximated as:

$$u(t) = U_0 + \frac{2}{n\pi}\sum_{n=1}^{N}\sin(2n\beta)\cos(2n\omega_s t) \quad (10)$$

0885-8977 (c) 2015 IEEE. Personal use is permitted, but republication/redistribution requires IEEE permission. See http://www.ieee.org/publications_standards/publications/rights/index.html for more information.

This article has been accepted for publication in a future issue of this journal, but has not been fully edited. Content may change prior to final publication. Citation information: DOI 10.1109/TPWRD.2015.2464323, IEEE Transactions on Power Delivery

where ω_s is the fundamental frequency of the system. We can approximate $u(t)$ as:

$$u(t) \approx U_0 + U_1 \cos 2\omega_s t \tag{11}$$

where $U_0 = \frac{2\beta}{\pi}$ and $U_1 = \frac{2}{\pi}\sin(2\beta)$

If the line current is considered as:

$$i_{line}(t) = -I_{line} \sin \omega_s t + \Delta i_{line}(t) \tag{12}$$

Then substituting Eq. (12) in Eq. (9) results in:

$$\begin{aligned} C_{fg}\frac{dv_C(t)}{dt} = (U_0 + U_1 \cos 2\omega_s t) \\ (-I_{line} \sin(\omega_s t) + \Delta i_{line}(t)) \end{aligned} \tag{13}$$

It is noted that the line current is considered to be purely sinusoidal; therefore, $\Delta i_{line}(t)$ in Eq. (12) is only due to sub or super-synchronous frequencies. These means that , in one hand, when the transmission line is not equipped with either series capacitor or the GCSC, $\Delta i_{line}(t) = 0$. On the other hand, in case of sub-synchronous oscillation, in addition to the fundamental frequency, the line current contains both sub-synchronous (ω_{SSR}) and super-synchronous (ω_{SupSR}) frequency components, and the $\Delta i_{line}(t)$ can be defined as [36]:

$$\Delta i_{line}(t) = -I_{SSR} \sin(\omega_{SSR} t) - I_{SupSR} \sin(\omega_{SupSR} t) \tag{14}$$

where ω_{SSR} and ω_{SupSR} are defined as follows:

$$\omega_{SSR} = 2\pi(f_s - f_n), \quad \omega_{SupSR} = 2\pi(f_s + f_n) \tag{15}$$

Based on the Eq. (13), two cases could be considered:

- Case I: $\Delta i_{line}(t) = 0$

Substituting Eq. (12), with $\Delta i_{line}(t) = 0$, in Eq. (13), and simplifying the equations, the fundamental component of $v_C(t)$ is obtained as:

$$v_{C1}(t) = V_{C1} \cos(\omega_s t) \tag{16}$$

where

$$V_{C1} = I_{line} X_{Cfg} \frac{(2\beta - \sin(2\beta))}{\pi} \tag{17}$$

Eq. (17) gives us the effective reactance of the GCSC given in Eq. (4).

- Case II: $\Delta i_{line}(t) \neq 0$

In this case, substituting Eq. (14) in Eq. (13) results in:

$$\begin{aligned} C_{fg}\frac{dv_C(t)}{dt} = (U_0 + U_1 \cos 2\omega_s t) \\ (-I_{line} \sin(\omega_s t) - I_{SSR} \sin(\omega_{SSR} t) \\ -I_{SupSR} \sin(\omega_{SupSR} t)) \end{aligned} \tag{18}$$

Using Eq. (18), the perturbation in the GCSC voltage resulting from sub-synchronous components is obtained from:

$$\begin{aligned} C_{fg}\frac{d\Delta v_C(t)}{dt} = (U_0 + U_1 \cos 2\omega_s t). \\ (-I_{SSR} \sin(\omega_{SSR} t) - I_{SupSR} \sin(\omega_{SupSR} t)) \end{aligned} \tag{19}$$

Simplifying Eq. (19), ignoring the high frequency components, and considering only the sub-synchronous and super-synchronous components will result in (see Appendix for the proof):

$$\begin{aligned} \Delta v_C(t) &= \frac{1}{C_{fg}\omega_{SSR}}(U_0 I_{SSR} - \frac{U_1}{2} I_{SupSR}) \cos(\omega_{SSR} t) \\ &+ \frac{1}{C_{fg}\omega_{SupSR}}(-\frac{U_1}{2} I_{SSR} \\ &+ U_0 I_{SupSR}) \cos(\omega_{SupSR} t) \\ &= V_{SSR} \cos(\omega_{SSR} t) + V_{SupSR} \cos(\omega_{SupSR} t) \end{aligned} \tag{20}$$

Using Eq. 20, V_{SSR}, V_{SupSR}, I_{SSR}, and I_{SupSR} can be related using the following matrix:

$$\begin{bmatrix} V_{SSR} \\ V_{SupSR} \end{bmatrix} = \begin{bmatrix} \frac{U_0}{C_{fg}\omega_{SSR}} & -\frac{U_1}{2C_{fg}\omega_{SSR}} \\ \frac{U_1}{2C_{fg}\omega_{SupSR}} & \frac{U_0}{C_{fg}\omega_{SupSR}} \end{bmatrix} \begin{bmatrix} I_{SSR} \\ I_{SupSR} \end{bmatrix} \tag{21}$$

If we name the 2×2 matrix in Eq. (21) as matrix A, then the determinant of this matrix can be expressed as:

$$det(A) = \frac{\omega_s^2 X_{Cfg} X_G (2\beta + \sin 2\beta)}{\pi \omega_{sub} \omega_{sup}} \tag{22}$$

It is obvious from Eq. (22) that the determinant is always positive; therefore, the GCSC presents a capacitive response.

If we approximate $I_{SupSR} \approx 0$, then Eq. (21) can be written as:

$$V_{SSR} = \frac{1}{C_{fg}\omega_{SSR}} U_0 I_{SSR} \tag{23}$$

Using Eq. (4), the GCSC's effective capacitance can be expressed as:

$$C_G = \frac{\pi C_{fg}}{2\beta - \sin 2\beta} \tag{24}$$

Substituting U_0 in Eq. (23) and using Eq. (24) results in:

$$V_{sub} = \frac{1}{C_{fg}\omega_{sub}} \frac{2\beta}{\pi} I_{sub} = \frac{1}{C_{SSR}\omega_{sub}} I_{sub} \tag{25}$$

where

$$C_{SSR} = C_G(1 - \frac{\sin 2\beta}{2\beta}) \tag{26}$$

Eq. (26) shows that the effect of the GCSC in SSR damping is to modify the effective capacitance of the GCSC from C_{GCSC} to C_{SSR}, which determines the resonance. Therefore, compared to a fixed capacitor, the SSR mitigation using a GCSC is limited to changing the resonance frequency, which may not be sufficient. Hence, an auxiliary SSR damping controller (SSRDC) should be added to the GCSC controller to enable the GCSC to damp the SSR.

0885-8977 (c) 2015 IEEE. Personal use is permitted, but republication/redistribution requires IEEE permission. See http://www.ieee.org/publications_standards/publications/rights/index.html for more information.

This article has been accepted for publication in a future issue of this journal, but has not been fully edited. Content may change prior to final publication. Citation information: DOI 10.1109/TPWRD.2015.2464323, IEEE Transactions on Power Delivery

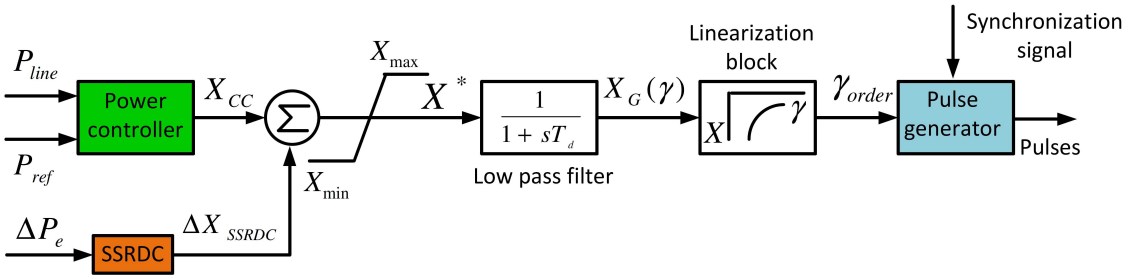

Fig. 8. Block diagram of the GCSC controller.

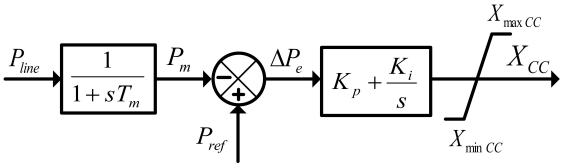

Fig. 9. Block diagram of the GCSC power scheduling controller (PSC).

IV. Control of GCSC

In this paper, the GCSC controller composed of a power scheduling controller (PSC) and an auxiliary SSRDC, as shown in Fig. 8.

A. GCSC Power Scheduling Controller

The duty of the PSC is to adjust the GCSC reactance in order to meet the required steady state power flow requirements of the transmission line. The block diagram of the GCSC PSC is shown in Fig. 9. In this figure, T_m is the time constant of the first order low pass filter associated with the measurement of the line current. In this controller, the measured line power is compared to a reference power, and the error is passed through a proportional-integral (PI) regulator.

B. Sub-Synchronous Resonance Damping Control

In order to enhance the SSR damping, an auxiliary SSRDC is added to the GCSC control system with an appropriate input control signal. Fig. 10 shows the SSRDC designed for the GCSC. The SSRDC consists of a gain block, a signal washout block, a two-stage phase compensation blocks, and a limiter block. The output of the SSRDC goes to the power controller of the GCSC to modulate the GCSC reactance. It is preferred the control signal to be local to avoid the effect of communication delay. In this paper, the line's real power is used as the control signal. The control signal is passed through a washout control block, which is a high pass filter, to avoid affecting the system's steady state operation. The value of T_W is high enough, $10\ sec.$, to allow signals associated with the oscillation in the input to pass without any changes. The two-stage phase compensation block is to enhance the dynamic system response. The GCSC controller parameters, i.e. K_p, K_i, K_{PSSR}, T_1, T_2, T_3, and T_4 are optimized using genetic algorithm (GA) to search for the optimal values of the design variables in order to achieve the fastest settling time and less over-shoot. The GA has the ability to derive the global optimum solution with relative computational simplicity even in the case of complicated problems [37]. The objective function (OF) is an integral of time multiplied absolute value of the real power deviation, which is expressed as Eq. (27). The goal is to minimize the OF to enhance the system dynamic response.

TABLE I
Constraints values and optimized parameters of the GCSC controller using GA.

Parameter	Min. value	Max. value	Optimum value
K_i	$1e-4$	10	0.15
K_p	$1e-4$	10	1.00
K_{PSSR}	$1e-4$	200	0.065
T_1	$1e-4$	10	0.018
T_2	$1e-4$	10	0.054
T_3	$1e-4$	10	1.581
T_4	$1e-4$	10	0.008

$$OF = \int_0^{t_{sim}} \mathrm{t}|\Delta \mathrm{P_e}|\,\mathrm{d}t \tag{27}$$

where t_{sim} is the simulation time of $10\ sec.$.

The genetic algorithm block of the PSCAD program is used in order to find the controller parameters. This block is suitable for optimization of several real/integral/logical variables. In this block, an adaptive stochastic optimization algorithm involving search and optimization is used. An electronic organism as a binary string (chromosome) is created and then genetic and evolutionary principles of fitness-proportionate selection for reproduction (including random crossover and mutation) are used to find extremely large solution spaces efficiently [38].

The parameters of the GCSC controllers obtained by GA and the corresponding constraints are given in Table I.

V. Results and Discussion

In this section, the effectiveness of the GCSC with SSRDC in SSR mitigation is verified using simulation results in PSCAD. Moreover, to compare the GCSC performance in SSR damping with other FACTS devices, its performance is compared to commercially available FACTS, thyristor controlled series capacitor (TCSC), using both time-domain simulation and time-frequency analysis.

0885-8977 (c) 2015 IEEE. Personal use is permitted, but republication/redistribution requires IEEE permission. See http://www.ieee.org/publications_standards/publications/rights/index.html for more information.

This article has been accepted for publication in a future issue of this journal, but has not been fully edited. Content may change prior to final publication. Citation information: DOI 10.1109/TPWRD.2015.2464323, IEEE Transactions on Power Delivery

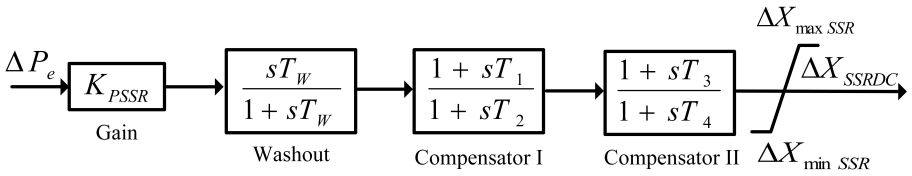

Fig. 10. SSRDC block diagram.

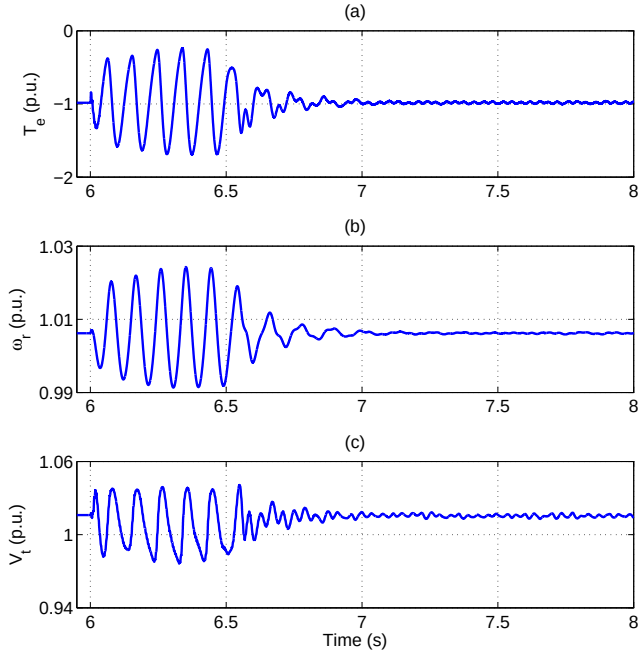

Fig. 11. Wind farms response with and without SSRDC (a) Electric torque (b) Rotor speed (c) IG terminal voltage.

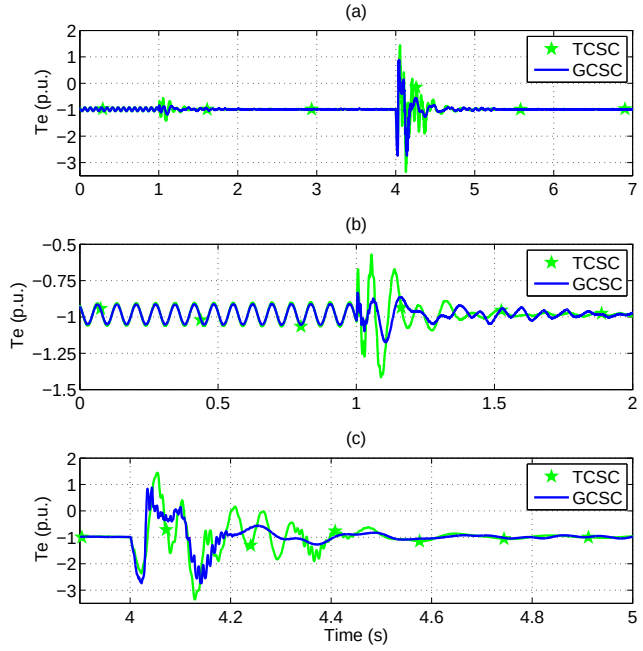

Fig. 12. Electric torque response due to IGE with TCSC and GCSC (a) results from 0 to 10 $sec.$, (b) results from 0 to 2 $sec.$, and (c) results from 3.9 to 5 $sec.$

A. Simulation Results with and without SSRDC

The GCSC performance in SSR damping is evaluated considering the worst operating condition of the wind farm, i.e. 70% series compensation. In order to verify that the GCSC requires a SSRDC to mitigate the SSR, the wind farm is started with 30% fixed series compensation, and then at t = 6 $sec.$, the GCSC- with the compensation level of 70% and without SSRDC, is replaced with the fixed series capacitor. Afterwards, at t = 6.5 $sec.$, the GCSC is equipped with the SSRDC. Fig. 11 shows the dynamic response of the wind farm, including electric torque, rotor speed, and IG terminal voltage for the aforementioned situation. As seen in this figure, as soon as the 30% fixed compensation is replaced with a GCSC without SSRDC, undamped SSR frequencies appear in the system, showing that a GCSC without a SSRDC is unable to damp the SSR, as was expected according to what explained in Section III-B. However, when the SSRDC is added to the GCSC, the SSR in the system is damped, and the wind farm becomes stable.

B. Performance Comparison of GCSC and TCSC

The TCSC has been adopted for SSR damping, power-flow control, and real power oscillation damping in numerous examples of practical applications [36]. In this paper, in order to verify the effectiveness of the GCSC in SSR damping, its performance is compared with the TCSC.

The TCSC and GCSC performance in the SSR damping is evaluated when the series compensation level provided by the GCSC and TCSC is 70%. For a fair comparison , the SSRDC of the TCSC has similar topology to that of the GCSC, as shown in Fig. 10, and it is designed and optimized in similar fashion as GCSC. In this comparison, the wind farm starts with a 70% fixed series compensation, at which the system is unstable. Then at t = 1 $sec.$, the GCSC and TCSC are activated, and at t = 4 $sec.$, a 3LG short circuit with duration of 75 $msec.$ is applied at point B in Fig. 1. Figs. 12 through 14 compare the series-compensated wind farm electric torque, the IG speed, and the IG terminal RMS voltage with the GCSC and the TCSC. In these figures, since the wind farm starts with a compensation level at which the wind farm is unstable, the wind farm tends to go unstable, as seen in more detail in Fig. 12 (b), until the FACTS devices are activated at t = 1 $sec.$

0885-8977 (c) 2015 IEEE. Personal use is permitted, but republication/redistribution requires IEEE permission. See http://www.ieee.org/publications_standards/publications/rights/index.html for more information.

This article has been accepted for publication in a future issue of this journal, but has not been fully edited. Content may change prior to final publication. Citation information: DOI 10.1109/TPWRD.2015.2464323, IEEE Transactions on Power Delivery

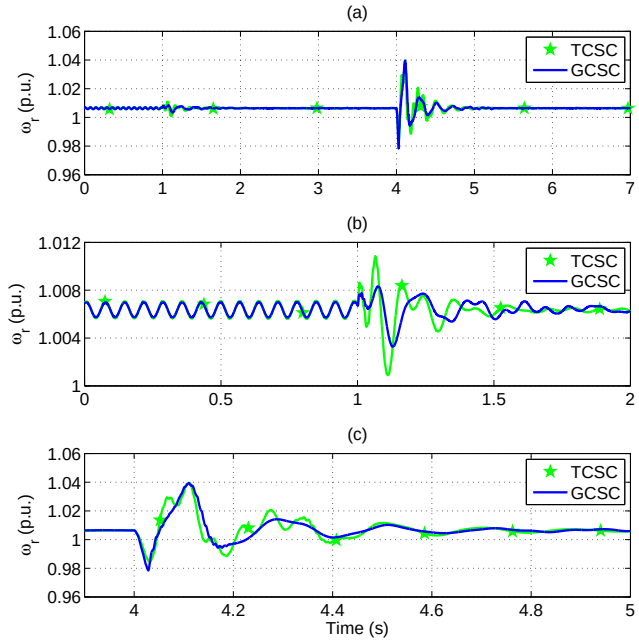

Fig. 13. IG rotor speed response due to IGE with TCSC and GCSC (a) results from 0 to 10 $sec.$,(b) results from 0 to 2 $sec.$, and (c) results from 3.9 to 5 $sec.$

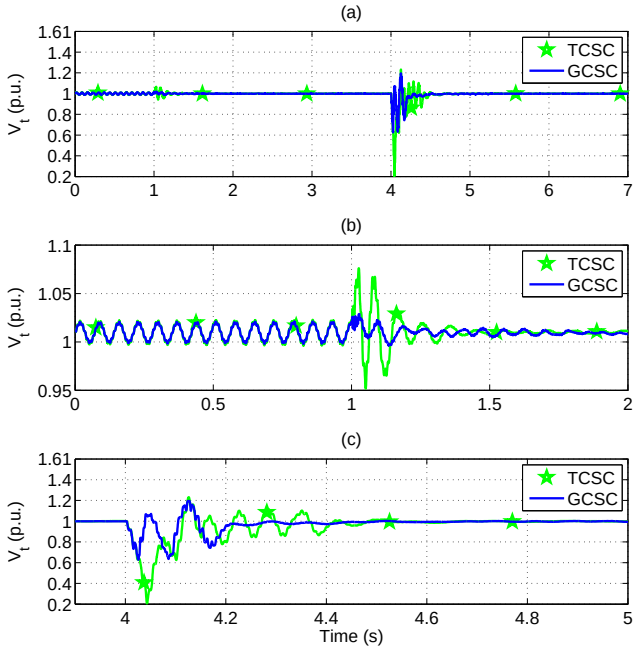

Fig. 14. IG terminal RMS voltage response due to IGE with TCSC and GCSC (a) results from 0 to 10 $sec.$,(b) results from 0 to 2 $sec.$, and (c) results from 3.9 to 5 $sec.$

Comparing the TCSC and GCSC results in SSR damping by looking at the wind farms electric torque, as shown in Fig. 12, reveals that the SSR is damped in case of GCSC in less than 0.2 $sec.$ from the initiation of the fault. The same figure also shows that in case of the TCSC compensation, the SSR lasts approximately 0.2 $sec.$ longer than the GCSC's response, and it takes 0.4 $sec.$ to be mitigated in the wind farm. Figs. 13 and 14 show a similar behavior as Fig. 12. A more detailed comparison is given in following section.

C. Time-Frequency Analysis of the SSR

The time-varying frequency characteristic of a non-stationary signal such as SSR can be best described by time-frequency analysis [31]. Any time-frequency distribution (TFD) can be obtained from Cohen's class equation as follows [30]:

$$TFD_x(t,\omega;\phi) = \frac{1}{4\pi^2}\int\int\int x^*(u-\frac{\tau}{2})x(u+\frac{\tau}{2}) \times\phi(\theta,\tau)e^{-j\theta t-j\tau\omega+j\theta u}d\theta d\tau du \quad (28)$$

We employed the most suitable kernel reduced interference distribution to analyze and quantify the time-varying frequency content of the SSR presented in this paper. The kernel satisfies the time- and frequency marginal properties as follows [30]:

$$\int TFD_x(t,\omega;\phi)d\omega = |x(t)|^2,\ if\ \phi(\theta,\tau=0)=1 \quad (29)$$

$$\int TFD_x(t,\omega;\phi)dt = |X(\omega)|^2,\ if\ \phi(\theta=0,\tau)=1 \quad (30)$$

where Eqs. (29) and (30) are known as the time marginal and frequency marginal, respectively. As seen in the marginal equations, the TFD provides the absolute-value squared time-domain signal for time marginal and absolute value squared Fourier transform for the frequency marginal. Based on the time-marginal property of the TFD, the Instantaneous Distortion Energy (IDE) [31] can be utilized for the quantification of the SSR damping. The IDE is basically the ratio of the energy of the disturbance to the energy of the fundamental frequency component and is defined as [31]:

$$IDE(t) = \sqrt{\frac{\int TFD_D(t,\omega;\phi)d\omega}{\int TFD_F(t,\omega;\phi)d\omega}} \times 100\% \quad (31)$$

In addition, from the frequency marginal property, one can obtain the maximum energy, i.e. (E_{max}), at the SSR frequency as follows [31]:

$$E_{max} = max\left\{\int TFD_x(t,\omega;\phi)dt\right\} = max\{|x(\omega)|^2\} \quad (32)$$

In Fig. 15, the plots from top to bottom are called (a), (b), (c) and (d), respectively, where (a) is the line current, (b) is the transient part of the line current that is separated from the fundamental frequency, (c) is the time-frequency distribution of (b), and (d) is the IDE of the line current. Without FACTS is installed in the line, as shown in Fig. 15-A-(b), the transient part of the line current does not disappear and persists in the system even after the fault is cleared. Also, Fig. 15-A-(c) shows that, following the fault, some super- and sub-synchronous frequencies occur in the line current. The energy level of super-synchronous frequency, between 60 and 65 Hz, is quite low, and it damps out very fast after about 0.4 $sec.$ However, the most dominant sub-synchronous frequency with

0885-8977 (c) 2015 IEEE. Personal use is permitted, but republication/redistribution requires IEEE permission. See http://www.ieee.org/publications_standards/publications/rights/index.html for more information.

This article has been accepted for publication in a future issue of this journal, but has not been fully edited. Content may change prior to final publication. Citation information: DOI 10.1109/TPWRD.2015.2464323, IEEE Transactions on Power Delivery

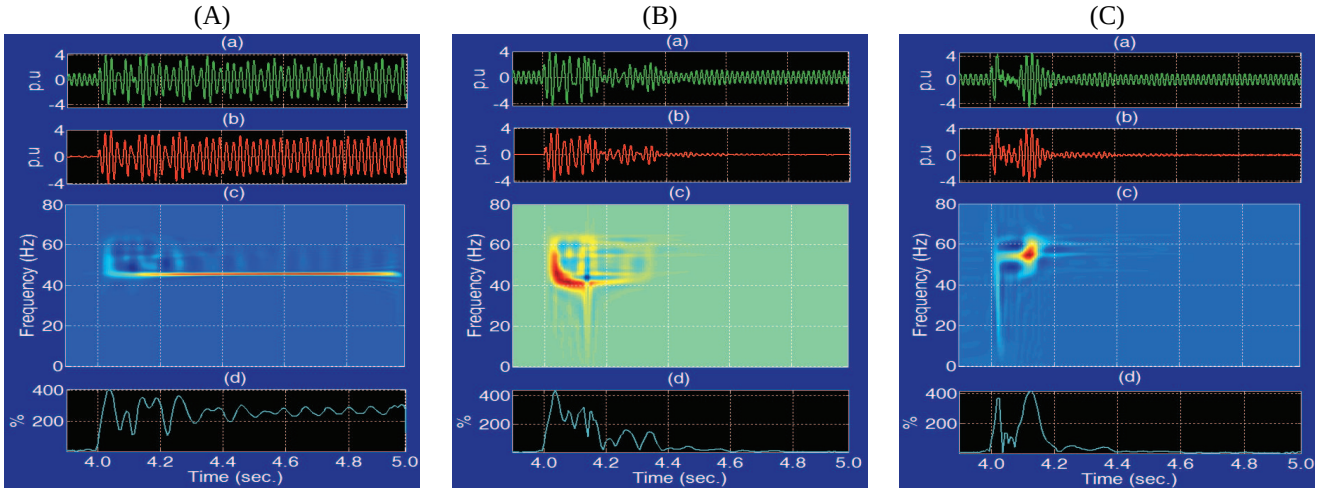

Fig. 15. Time-frequency analysis of line current; (A) without FACTS, (B) with TCSC, and (C) with GCSC.

the highest energy concentration does not damp out and exists in the line current even after the fault is cleared, indicating instability of the wind farm. In addition, Fig. 15-A-(d) shows that the IDE of the line current does not return to zero, and it is sustained at approximately 250%.

Fig. 15-B shows the time-frequency analysis of the wind farm instantaneous line current with the TCSC. As shown in Fig. 15-B-(b), the transient part of the line current goes to zero at approximately $0.4\ sec.$ after the fault is cleared. Time frequency distribution of Fig. 15-B-(b), represented in Fig. 15-B-(c), reveals that after the fault some super- and sub-synchronous resonances with the frequency range of 30 to 70 Hz are generated in the line current. However, $0.4\ sec.$ after the fault, both super- and sub-synchronous resonances disappear from the line current. Finally, Fig. 15-B-(d) shows that the IDE of the system goes to zero $0.6\ sec.$ after the fault.

Fig. 15-C shows the time-frequency analysis of the wind farm instantaneous line current with the GCSC. In this case, the transient component of the line current goes to zero about $0.2\ sec.$ after the instance of initiation of the fault. Time frequency distribution represented in Fig. 15-C-(c) shows that, after the fault, some super- and sub-synchronous resonances with the frequency range of 30 to 65 Hz are presented in the line current. In case of the GCSC, $0.2\ sec.$ after the fault, both super- and sub-synchronous resonances disappear from the line current, verifying the effectiveness of the GCSC in SSR damping in wind farms. In Fig. 15-C-(d) the IDE of the system goes to zero $0.4\ sec.$ after the fault which indicates the stability of the system.

One can quantify the maximum energy content of the SSR frequencies, i.e. the E_{max}, according to the Eq. 32. Also, a higher E_{max} indicates the longer existence of the SSR frequencies in the line current disturbance. When no FACTS is installed, the E_{max} was calculated 1574.00. Also, for the TCSC and the GCSC these values are found to be 169.10 and 161.70, respectively. This result shows that the GCSC has lower E_{max} compared to that of the TCSC, indicating that the SSR frequencies exist in the line current disturbance in a shorter time when the FSWTGS is equipped with a GCSC. This shows the superior performance of the GCSC compared to the TCSC.

VI. Conclusion

In this paper, we have proposed the application and control of the gate-controlled series capacitor (GCSC) for series compensation and SSR mitigation in fixed-speed wind turbine generator systems (FSWTGS). Not all the wind farms will exhibit SSR problems by use of modern power electronic devices; however, in wind farms with fixed-speed generators, the SRR may be a potential risk for grid interconnection, if the level of compensation is not well-controlled. Thus, in our investigation, the series compensation is tuned such that the magnitude of the equivalent negative rotor resistance exceeds the sum of the positive resistances of the armature and the power network.

It is shown that the power scheduling controller (PSC) of the GCSC is not adequate to damp the SSR. Therefore, a SSR damping controller (SSRDC) is designed and added to the power controller control to enable the GCSC to damp the SSR. In order to verify the effectiveness of the GCSC in SSR damping, its performance is compared with a well-known and commercially available series FACTS device, thyristor-controlled series capacitor (TCSC).

Unlike the TCSC that may present the problem of an internal resonance due to its parallel capacitor and inductor, which limits the TCSC's operating area, the GCSC provides a fully controllable continues capacitive impedance without the risk of an internal resonance. Moreover, a comparison of the rating of the TCSC and the GCSC components, when both the GCSC and TCSC have the same maximum capacitive impedance, shows that the power ratings of the GCSC capacitor and power electronics switches are smaller than that of the TCSC [39].

Having the performance comparison results of the GCSC and TCSC presented in this paper, and also considering the component rating comparison of the TCSC and GCSC presented in [39], it seems that the GCSC is a potential solution for series compensation of FSWTGS. In this paper, we investigated design and application of GCSC, which is not

0885-8977 (c) 2015 IEEE. Personal use is permitted, but republication/redistribution requires IEEE permission. See http://www.ieee.org/publications_standards/publications/rights/index.html for more information.

This article has been accepted for publication in a future issue of this journal, but has not been fully edited. Content may change prior to final publication. Citation information: DOI 10.1109/TPWRD.2015.2464323, IEEE Transactions on Power Delivery

yet fully investigated compared to TCSC, and we believe that the GCSC can provide alternative technical solutions for next-generation electric power systems transient stability issues.

APPENDIX

In this Appendix, the proof of Eq. (20) is given. Expanding (Eq. 19) will result in:

$$\begin{aligned} C_{fg}\frac{d\Delta v_C(t)}{dt} = &-I_{SSR}U_o\sin(\omega_{SSR}t) \\ &- I_{SupSR}U_o\sin(\omega_{SupSR}t) \\ &- I_{SSR}U_1\sin(\omega_{SSR}t)\cos(2\omega_s t) \\ &- I_{SupSR}U_1\sin(\omega_{SupSR}t)\cos(2\omega_s t) \end{aligned} \tag{33}$$

Extending again Eq. (33), we will have:

$$\begin{aligned} C_{fg}\frac{d\Delta v_C(t)}{dt} = &-I_{SSR}U_o\sin(\omega_{SSR}t) \\ &- I_{SupSR}U_o\sin(\omega_{SupSR}t) \\ &- \frac{I_{SSR}U_1}{2}\Bigg(\sin\Big(\omega_{SSR}+2\omega_s\Big)t+\sin\Big(\omega_{SSR} \\ &- 2\omega_s\Big)t\Bigg) - \frac{I_{SupSR}U_1}{2}\Bigg(\sin\Big(\omega_{SupSR} \\ &+ 2\omega_s\Big)t + \sin\Big(\omega_{SupSR} - 2\omega_s\Big)t\Bigg) \end{aligned} \tag{34}$$

We have defined the following equations in the paper:

$$\omega_{SSR} = 2\pi(f_s - f_n) = \omega_s - \omega_n \tag{35}$$

$$\omega_{SupSR} = 2\pi(f_s + f_n) = \omega_s + \omega_n \tag{36}$$

where f_n is electric natural frequency of the system as defined in the paper (see Eq. (1).)

Using Eqs. (35) and (36):

$$\omega_{SSR} - 2\omega_s = -\omega_{SupSR} \quad \omega_{SupSR} - 2\omega_s = -\omega_{SSR} \tag{37}$$

Substituting Eq. (37) into Eq. (34) and considering only the sub-synchronous and super-synchronous components will result in Eq. (20).

REFERENCES

[1] P. Mitra, Lidong Zhang, L. Harnefors, "Offshore wind integration to a weak grid by VSC-HVDC links using power-synchronization control: a case study," *IEEE Trans. Power Delivery*, vol. 29, no. 1, pp. 453 - 461, Feb. 2014.

[2] Z. Wang, B. Yuwen, Y. Lang, M. Cheng, "Improvement of Operating Performance for the Wind Farm With a Novel CSC-Type Wind Turbine-SMES Hybrid System," *IEEE Trans. Power Delivery*, vol. 28, no. 2, pp.693 - 703, April 2013.

[3] S. Lumbreras, A. Ramos, T. Isobe, R. Shimada, "Optimal design of the electrical layout of an offshore wind farm applying decomposition strategies," *IEEE Trans. Power Systems*, vol. 28, no. 2, pp. 1434-1441, May 2013.

[4] N. R. Chaudhuri, B. Chaudhuri, "Considerations Toward Coordinated Control of DFIG-Based Wind Farms," *IEEE Trans. Power Delivery*, vol. 28, no. 3, pp.1263 - 1270, July 2013.

[5] L. Wang, D. N. Truong,"Comparative stability enhancement of PMSG-based offshore wind farm fed to an SG-based power system using an SSSC and an SVeC," *IEEE Trans. Power Systems*, vol. 28, no. 2, pp. 1336-1344, May 2013.

[6] A. Sumper, O. Gomis-Bellmunt, A. Sudria-Andreu, R. Villafafila-Robles, J. Rull-Duran, "Response of fixed speed wind turbines to system frequency disturbances," *IEEE Trans. Power Systems*, vol. 24, no. 1, pp. 181-192, February 2009.

[7] "Series compensation: boosting transmission capacity," http://www.abb.com/FACTS.

[8] S. Golshannavaz, S. Aminifar, D. Nazarpour, "Application of UPFC to enhancing oscillatory response of series-compensated wind farm integrations," *IEEE Trans. Smart Grid*, vol. 5, no. 4, pp. 1961 - 1968, July 2014.

[9] IEEE SSR Working Group, "Terms, definitions and symbols for subsynchronous oscillations," *IEEE Trans. Power Appl. Syst.* PAS-104, pp. 1326-1334, June 1985.

[10] K. R. Padiar, Analysis of sub-synchronous resonance in power systems, Kluwer Academic Publishers (KAP), Boston, 1999.

[11] L. Fan, Z. Miao, "Mitigating SSR using DFIG-based wind generation," *IEEE Trans. Sustainable Energy*, vol. 3, no. 3, pp. 349-358, July 2012.

[12] L. Fan, R. Kavasseri, Z. Miao, C. Zhu, "Modeling of DFIG-based wind farms for SSR Analysis," *IEEE Trans. Power Delivery*, vol. 25, no. 4, pp. 2073-2082, October 2010.

[13] L. Fan, C. Zhu, Z. Miao, M. Hu, "Modal analysis of a DFIG-based wind farm interfaced with a series compensated network," *IEEE Trans. Energy Conversion*, vol. 26, no. 4, pp. 1010 - 1020, Dec. 2011.

[14] S. O. Faried, I. Unal, D. Rai, J. Mahseredjian, "Utilizing DFIG-based wind farms for damping subsynchronous resonance in nearby turbine-generators," *IEEE Trans. Power Systems*, vol. 28, no. 1, pp. 452 - 459, Feb. 2013.

[15] M. S. El-Moursi, B. Bak-Jensen, M. H. Abdel-Rahman, "Novel STATCOM controller for mitigating SSR and damping power system oscillations in a series compensated wind park," *IEEE Trans. Power Electronics*, vol. 25, no. 2, pp. 429 - 441, Feb. 2010.

[16] S. Golshannavaz, M. Mokhtari, D. Nazarpour, "SSR suppression via STATCOM in series compensated wind farm integrations," *2011 19th Iranian Conference on Electrical Engineering (ICEE)*, 17 - 19 May 2011.

[17] E. Santacana et al., "Power to be efficient: transmission and Distribution Technologies are the Key to Increased Energy Efficiency," ABB Review Feb. 2007.

[18] "http://www.abb.com/search.aspx?q=TCSC"

[19] K. R. Padiyar, FACTS CONTROLLERS in Power Transmission and Distribution, New Age International (P) Ltd., 2007.

[20] F. D. de Jesus, E. H. Watanabe, L. F. W. de Souza, J. E. R. Alves, "SSR and power oscillation damping using gate-controlled series capacitors (GCSC)," *IEEE Trans. Power Delivery*, vol. 22, no. 3, pp. 1806 - 1812, July 2007.

[21] E. H. Watanabe, L. F. W. de Souza, F. D. de Jesus, J. E. R. Alves, A. Bianco, "GCSC - gate controlled series capacitor: a new FACTS device for series compensation of transmission lines," *2004 IEEE/PES on Transmission and Distribution Conference and Exposition: Latin America*, pp. 981 - 986, 8-11 Nov. 2004.

[22] F. D. de Jesus, E. H. Watanabe, L. F. W. Souza, J. E. R. Alves, "SSR mitigation using gate-controlled series capacitors," *IEEE Power Engineering Society General Meeting*, 2006.

[23] H. A. Mohammadpour, S. M. H. Mirhoseini, A. Shoulaie, "Comparative study of proportional and TS fuzzy controlled GCSC for SSR mitigation," *International Conference on Power Engineering, Energy and Electrical Drives, 2009. POWERENG '09*, pp. 564 - 569, 18 - 20 March 2009.

[24] M. Pahlavani, H. A. Mohammadpour, "Damping of sub-synchronous resonance and low-frequency power oscillation in a series-compensated transmission line using gate-controlled series capacitor," *Electric Power Systems Research*, vol. 81, Issue 2, pp. 308-317, February 2011.

[25] H. A. Mohammadpour, Md. Moinul Islam, D. Coats, E. Santi, Y. J. Shin, "Sub-synchronous resonance mitigation in wind farms using gate-controlled series capacitor," *IEEE 4th International Symposium on Power Electronics for Distributed Generation Systems (PEDG) 2013*, pp. 1 - 6, 8 - 11 July, Rogers, AR, USA.

[26] IEEE SSR Task Force, "First benchmark model for computer simulation of subsynchronous resonance," *IEEE Trans. Power App. Syst.*, vol. PAS-96, pp. 1562-1572, Sep./Oct. 1997.

[27] EMTDC PSCAD User Manual, HVDC Research Center, Winnipeg, MB, Canada, 2005.

[28] M. Mokjhtari, J. Khazaie, and D. Nazarpour, "Sub-synchronous resonance damping via doubly fed induction generator," *Electrical Power and Energy Systems*, vol. 53, no. 1, pp. 876 - 883, December 2013.

[29] A. Ghorbani, S. Pourmohammad, "A novel excitation controller to damp subsynchronous oscillations," *Electrical Power and Energy Systems*, vol. 33, no. 3, pp. 411 - 419, March 2011.

0885-8977 (c) 2015 IEEE. Personal use is permitted, but republication/redistribution requires IEEE permission. See http://www.ieee.org/publications_standards/publications/rights/index.html for more information.

This article has been accepted for publication in a future issue of this journal, but has not been fully edited. Content may change prior to final publication. Citation information: DOI 10.1109/TPWRD.2015.2464323, IEEE Transactions on Power Delivery

[30] L. Cohen, *Time-frequency signal analysis*, Prentice Hall, New York, 1995.
[31] Y. J. Shin, E. J. Powers, W. M. Grady, A. Arapostathis, "Power quality indices for transient disturbances," *IEEE Trans. Power Delivery*, vol. 21, no. 1, pp. 253 - 261, January 2006.
[32] Y. J. Shin, E. J. Powers, A. Arapostathis, "Signal Processing-Based Direction Finder for Transient Capacitor Switching Disturbances," *IEEE Trans. Power Delivery*, vol. 23, no. 4, pp. 2555 - 2562, October 2008.
[33] V. Akhmatova, H. Knudsenb, "An aggregate model of a grid-connected, large-scale, offshore wind farm for power stability investigations importance of windmill mechanical system," *International Journal of Electrical Power and Energy Systems*, vol. 24, Issue 9, pp. 709 - 717, November 2002.
[34] E. Levi and D. Rauski, "Modeling of deep-bar and double cage self-excited induction generators for wind-electricity generation studies, Electr. Power Syst. Res., vol. 27, no. 1, pp. 7381, May 1993.
[35] S. J. Chapman, Electric Machinery Fundamentals, 4th ed. Toronto, ON, Canada: McGraw-Hill, 2005.
[36] N. G. Hingorani, L. Gyugi, *Understanding FACTS*, IEEE Press, April, 2000.
[37] K. Y. Lee, M. A. El-Sharkawi, "Tutorial on modern heuristic optimization techniques with applications to power systems," *IEEE Power Engineering Society*, 2002.
[38] EMTDC PSCAD User Manual, HVDC Research Center, Winnipeg, MB, Canada, 2005.
[39] L.F.W. de Souza, E.H. Watanabe, J.E. da Rocha Alves, "Thyristor and gate-Controlled series capacitors: a comparison of components rating," *IEEE Trans. Power Delivery*, vol. 23, no. 2, pp. 899 - 906, April 2008.

Hossein Ali Mohammadpour (S'2009 - M'2015) received the B.Sc. and M.Sc. degrees all in electrical engineering power systems from the Iran University of Science and Technology (IUST), Tehran, Iran, in 2006 and 2009, respectively. He also received the Ph.D. degree in electrical engineering with focus on renewable energy systems from the University of South Carolina, Columbia, SC, USA, in December 2014, where he continued as a postdoctoral fellow until March 2015. Since March 2015, he has been with the NRG Renew, Scottsdale AZ, USA as a Senior Power Systems Engineer. His current research interests include power systems stability and control, micro-grid systems, photovoltaic, battery energy storage systems, and smart grid.

Md Moinul Islam (S'2009 - M'2015) received the B.Sc. in Electrical and Electronic Engineering from Bangladesh University of Engineering and Technology (BUET) in 2008, and the M.E. and PhD degrees in Electrical Engineering from University of South Carolina, Columbia, SC, USA in 2011 and 2014, respectively. His research interest includes power quality, renewable energy sources, and advanced digital signal processing.

Enrico Santi (S'90 - M'94 - SM'02) received the Dr. Ing. degree in electrical engineering from the University of Padua, Italy in 1988 and the M.S. and Ph.D. degrees from Caltech in 1989 and 1994, respectively. He worked as a senior design engineer at TESLAco from 1993 to 1998, where he was responsible for the development of various switching power supplies for commercial applications. Since 1998 he has been with the University of South Carolina where he is currently an associate professor in the electrical engineering department. His research interests include switched-mode power converters, advanced modeling and simulation of power systems, modeling and simulation of semiconductor power devices, control of power electronics systems..

Yong-June Shin (S'98 - SM'04) received the B.S. (Hons.) degree in electrical engineering at Yonsei University, Seoul, Korea, in 1996, the M.S. degree in electrical engineering and computer science from The University of Michigan, Ann Arbor, MI, USA, in 1997, and the Ph.D. degree in electrical and computer engineering from The University of Texas at Austin, Austin, TX, USA, in 2004. Upon his graduation, he joined the Department of Electrical Engineering, The University of South Carolina, Columbia, SC, USA, as an Assistant Professor. He was promoted to Associate Professor with tenure in 2011. He joined the School of Electrical and Electronic Engineering, Yonsei University, Seoul, Korea as Associate Professor in 2012. His current research interests are characterized by the application of novel digital-signal-processing techniques to a wide variety of important transient and nonlinear problems in smart electric power grids. Prof. Shin is a recipient of the United States National Science Foundation CAREER award in 2008, and the General Electric Korean-American Education Commission Scholarship.

0885-8977 (c) 2015 IEEE. Personal use is permitted, but republication/redistribution requires IEEE permission. See http://www.ieee.org/publications_standards/publications/rights/index.html for more information.